Dynamics of Populations of Planetary Systems
Proceedings IAU Colloquium No. 197, 2005
Z. Knežević and A. Milani, eds.

DOI: 10.1017/S1743921304008713

Collision orbits and phase transition for 2004 AS_1 at discovery

Jenni Virtanen, K. Muinonen, M. Granvik and T. Laakso

Observatory, University of Helsinki, P.O.Box 14, FIN-00014 Helsinki, Finland
email: jenni.virtanen@helsinki.fi

Abstract. We evaluate asteroid orbital uncertainties from the discovery night onwards using 6D orbit computation tools based on statistical techniques. In particular, we outline a new nonlinear Monte Carlo technique of phase-space sampling that helps us in assessing the nonlinear phase transition from extended orbital-element distributions to well-constrained ones as the observational arc and number of observations grows. We apply the statistical techniques for near-Earth asteroid 2004 AS_1 to examine the time evolution of the orbital uncertainties and to assess the asteroid impact risk immediately after discovery. We start with the technique of statistical ranging for exiguous data, continue with the phase-space sampling technique for moderate data, and conclude with the standard least-squares fit for extensive data.

Keywords. Celestial mechanics, methods: statistical, minor planets, asteroids.

1. Introduction

For more than a decade, impacts of asteroids have been recognised as a significant threat to humankind, comparable to other major natural disasters. Due to the active monitoring of the impact risk, several new objects having non-zero probabilities for an Earth impact within the next century are identified each year. The realization of this cosmic threat has motivated the development of several theoretical and computational tools for relatively short-term collision probability assessment (over timescales of decades). The backbone of collision probability computations is the assessment of orbital uncertainty of the given object. The orbital uncertainty evolves rapidly after an object has been discovered, typically decreasing when new observations roll in and increasing when follow-up observations have failed. Thus also the asteroid collision probability evolves when the observational arc and the number of observations grows and, in fact, for most of the discovered impactor candidates the probabilities for an Earth impact have been shown to vanish after days or weeks of observations after the discovery.

In Muinonen and Virtanen (2002), a nonlinear collapse was seen in the orbital uncertainties as a function of the improving accuracy of astrometric observations. This phase transition effect can also be recognized in the time evolution of the orbital uncertainty: there is a threshold for the length of the observational arc (and the number of observations) over which the orbital-element distributions nonlinearly evolve from extended to well-constrained ones.

Most of the theoretical and computational work for collision probability assessment, such as that by Yeomans and Chodas (1994) and Chodas and Yeomans (1996, 1999), is however bounded by the use of linear approximation which has been shown to fail for short observational arcs. Milani and Valsecchi (1999) and Milani et al. (1999; 2000a, b, c) have made use of both linear and semilinear methods for the propagation of orbital uncertainty

(Milani 1999). They illustrate the probability of a collision with virtual impactors (for a review paper, see Milani 2004, this Proceedings).

We attack the problem of impact risk assessment at the very moment of discovery. The ill-posedness of this problem stems from the inverse problem of computing the orbit from a small number of observations covering a short observational arc. With statistical orbit computation techniques, the probability density of the orbital parameters, and in turn the collision probability, can be evaluated rigorously even for exiguous data, although the strict probabilistic interpretation of inversion results may be in doubt. Information on the orbital characteristics of the object, such as the minimum encounter distance with the planets in the near future, can nevertheless be extracted. To stress this ambivalence, in this paper we use the term "collision probability" only in connection to purely theoretical work, for practical purposes we replace it with the term "collision risk".

We provide a continuum of statistical orbit computation techniques that can be applied sequentially accounting for the phase transition effect. In particular, we outline an innovative 6D technique for asteroids with moderate time arcs and/or moderate numbers of observations. The technique of sampling in phase-space volume of variation makes use of local linear approximations by varying one or more orbital elements and fitting the remaining ones. The use of the curve (or line) of variation in evaluation of orbital uncertainties has already been brought up by Bowell *et al.* (1993) and Milani (1999), and has thereafter been used extensively by Milani in several application, such as ephemeris prediction, asteroid linkage, and collision probability assessment. We generalize the concept from a line to a volume of variation, and introduce Monte Carlo sampling in the phase-space volume for a fully nonlinear treatment.

We apply the orbit computation scheme to the case of 2004 AS1, an NEO discovered in early 2004 having a significant risk for a collision with the Earth some 48 hours following the discovery moment. While the risk of the immediate impact was removed with observations from the second night, the extreme nature of the first prediction calls for a detailed analysis.

2. Orbit computation

2.1. *Inverse problem*

We denote the osculating orbital elements of an asteroid at a given epoch t_0 by $\boldsymbol{P} = (a, e, i, \Omega, \omega, M_0)^T$ (T is transpose). The elements are, respectively, the semimajor axis, eccentricity, inclination, longitude of ascending node, argument of perihelion, and mean anomaly. The three angular elements i, Ω, and ω are currently referred to the ecliptic at equinox J2000.0.

The orbital-element probability density function (p.d.f.) $p_{\rm p}$ is proportional to the a priori ($p_{\rm pr}$) and observational error (p_ϵ) p.d.f.'s, the latter being evaluated for the sky-plane ("O-C") residuals $\Delta\boldsymbol{\psi}(\boldsymbol{P})$ (Muinonen and Bowell 1993),

$$p_{\rm p}(\boldsymbol{P}) \propto p_{\rm pr}(\boldsymbol{P}) p_\epsilon(\Delta\boldsymbol{\psi}(\boldsymbol{P})), \tag{2.1}$$

where p_ϵ can usually be assumed to be Gaussian. For the mathematical form of $p_{\rm p}$ to be invariant in transformations from one orbital element set to another (e.g., from Keplerian to equinoctial or Cartesian), we regularize the statistical analysis by Jeffreys' noninformative a priori p.d.f. (Jeffreys 1946, Muinonen *et al.* 2001),

$$\begin{aligned} p_{\rm pr}(\boldsymbol{P}) &\propto \sqrt{\det \Sigma^{-1}(\boldsymbol{P})}, \\ \Sigma^{-1}(\boldsymbol{P}) &= \Phi(\boldsymbol{P})^T \Lambda^{-1} \Phi(\boldsymbol{P}), \end{aligned} \tag{2.2}$$

https://doi.org/10.1017/S1743921304008713 Published online by Cambridge University Press

where Σ^{-1} is the information matrix (or the inverse covariance matrix) evaluated for the orbital elements $\boldsymbol{P}$, Φ contains the partial derivatives of right ascension (R.A.) and declination (Dec.) with respect to the orbital elements, and Λ is the covariance matrix for the observational errors. By the choice of the a priori p.d.f., the transformation of rigorous p.d.f.'s becomes analogous to that of Gaussian p.d.f.'s.

The final a posteriori orbital-element p.d.f. is

$$p_{\rm p}(\boldsymbol{P}) \propto \sqrt{\det \Sigma^{-1}(\boldsymbol{P})}\ \exp\left[-\frac{1}{2}\chi^2(\boldsymbol{P})\right],$$
$$\chi^2(\boldsymbol{P}) = \Delta\boldsymbol{\psi}^T(\boldsymbol{P})\Lambda^{-1}\Delta\boldsymbol{\psi}(\boldsymbol{P}). \tag{2.3}$$

As a consequence of securing the invariance in orbital-element transformations, e.g., ephemeris uncertainties and collision probabilities based on the orbital-element p.d.f. are independent of the choice of the orbital element set. Note that assuming constant $p_{\rm pr}$ is acceptable, when the exponent part of Eq. (2.3) confines the p.d.f. into a phase space regime, where the determinant part reduces to a constant (typical for well-constrained p.d.f.'s, i.e., long observational arcs). Note also that a predominating role of the a priori p.d.f. casts doubts upon the reliability of the probabilistic interpretation.

2.2. *Volume-of-variation sampling*

The a posteriori p.d.f. in Eq. (2.3) allows the derivation of a local linear approximation in the orbital-element phase space (Muinonen *et al.* 2004). We can select one or more elements as "the elements to be varied" systematically and derive a linear approximation for "the remaining elements to be fitted". For simplicity, we illustrate the local linear approximations below in the case of a single mapping element and note that the formulation is analogous for more numerous mapping elements.

We rewrite the a posteriori p.d.f. in Eq. (2.3) explicitly in terms of the mapping element $P_{\rm m}$ and the five remaining elements $\boldsymbol{P}'$ (here and below, the prime denotes five-dimensional quantities),

$$p_{\rm p}(P_{\rm m}, \boldsymbol{P}') \propto \sqrt{\det \Sigma^{-1}(P_{\rm m}, \boldsymbol{P}')} \cdot \exp\left[-\frac{1}{2}\chi^2(P_{\rm m}, \boldsymbol{P}')\right],$$
$$\chi^2(P_{\rm m}, \boldsymbol{P}') = \Delta\boldsymbol{\psi}^T(P_{\rm m}, \boldsymbol{P}')\Lambda^{-1}\Delta\boldsymbol{\psi}(P_{\rm m}, \boldsymbol{P}'). \tag{2.4}$$

For a given $P_{\rm m}$, we define the local linear approximation as follows,

$$p_{\rm p}(P_{\rm m}, \boldsymbol{P}') \propto \sqrt{\det \Sigma^{-1}(P_{\rm m}, \boldsymbol{P}'_{\rm ls})} \cdot \exp\left[-\frac{1}{2}\chi^2(P_{\rm m}, \boldsymbol{P}'_{\rm ls})\right] \cdot$$
$$\exp\left[-\frac{1}{2}\Delta\boldsymbol{P}'^T\Sigma'^{-1}(P_{\rm m}, \boldsymbol{P}'_{\rm ls})\Delta\boldsymbol{P}'\right],$$
$$\Delta\boldsymbol{P}' = \boldsymbol{P}' - \boldsymbol{P}'_{\rm ls}(P_{\rm m}), \tag{2.5}$$

where $\boldsymbol{P}'_{\rm ls} = \boldsymbol{P}'_{\rm ls}(P_{\rm m})$ is the local least-squares solution for the elements $\boldsymbol{P}'$. The local 5×5 covariance matrix Σ' is recomputed at the local least-squares solution P' and defines a hyperellipsoid centered at these elements. Note that both Σ^{-1} and Σ'^{-1} enter the local linear approximations above. The sequence of orbital elements $P_{\rm m}, \boldsymbol{P}'_{\rm ls}(P_{\rm m})$ defines the line of variation in the orbital-element phase space. The local covariance matrix Σ' defines a hyperellipsoid centered at the local least-squares orbital elements,

$$\Delta\chi^2(\boldsymbol{P}') = \Delta\boldsymbol{P}'^T\Sigma'^{-1}\Delta\boldsymbol{P}' \ = \ \Delta\chi^2_0, \tag{2.6}$$

where $\Delta\chi^2_0$ is a constant. The boundaries of, for example, the commonly used 68.3 % or 95.4 % -probability hyperellipsoids are $\Delta\chi^2_0 \approx 5.89$ or $\Delta\chi^2_0 \approx 11.3$, respectively.

https://doi.org/10.1017/S1743921304008713 Published online by Cambridge University Press

It is convenient to express the differences $\Delta \boldsymbol{P}'$ in terms of the standard deviations $\sigma'_j = \sqrt{\Sigma'_{jj}}$ $(j = 1, \ldots, 5)$ and to utilize the dimensionless correlation matrix C'; with the help of the diagonal standard deviation matrix S',

$$\begin{aligned} \Delta \boldsymbol{Q}' &= S'^{-1} \Delta \boldsymbol{P}', \\ C' &= S'^{-1} \Sigma' S'^{-1}, \\ S'_{jk} &= \sigma'_j \, \delta_{jk}, \quad j, k = 1, \ldots, 6, \end{aligned} \tag{2.7}$$

where δ_{jk} is the Kronecker symbol. The hyperellipsoid is thus defined by

$$\Delta \boldsymbol{Q}'^T C'^{-1} \Delta \boldsymbol{Q}' = \Delta \chi_0^2, \tag{2.8}$$

where all the parameters are dimensionless. The eigenvalues λ'_j $(j = 1, \ldots, 5)$ for the correlation matrix C' are normalized variances along the principal axes of the hyperellipsoid, the directions of the axes being given by the orthonormal eigenvectors $\boldsymbol{X}'_j$,

$$C' \boldsymbol{X}'_j = \lambda'_j \mathbf{X}'_j, \quad j = 1, \ldots, 5. \tag{2.9}$$

Since C' is a real and symmetric matrix, the eigenproblem is readily solved via Jacobi transformations.

It is our goal to draw sample orbits from the rigorous orbital-element p.d.f. with the help of the local linear approximations. First, we specify the variation interval for the mapping element with the help of the covariance matrix Σ derived in the global linear approximation and emphasize that the variation interval must be subject to iteration. For example, one may utilize the one-dimensional 3σ variation interval as given by the linear approximation so that

$$P_{\rm m} \in [P_{\rm m,ls} - 3\sigma_{\rm m}, P_{\rm m,ls} + 3\sigma_{\rm m}], \tag{2.10}$$

where $P_{\rm m,ls}$ is the global least-squares value for the mapping element. Second, the remaining elements are sampled with the help of the local intervals of variation so that

$$\boldsymbol{P}' = \boldsymbol{P}'_{\rm ls}(P_{\rm m}) + \sum_{j=1}^{5} (1 - 2r_j) \cdot \sqrt{\Delta \tilde{\chi}^2 \lambda'_j(P_{\rm m})} S'(P_{\rm m,ls}) \boldsymbol{X}'_j(P_{\rm m}), \tag{2.11}$$

where $r_j \in (0, 1)$ $(j = 1, \ldots, 5)$ are independent uniform random deviates and $\Delta \tilde{\chi}^2$ is a scaling parameter to be iterated so that the entire orbit solution space is covered and the final results have converged. Initially, one may start with $\Delta \tilde{\chi}^2 = 11.3$ and slowly increase its value. $S'(P_{\rm m,ls})$ designates the single standard deviation matrix used throughout the interval of the mapping parameter, which allows a straightforward debiasing of the sample orbits at the end of the computation.

In Eq. (2.11), we sample the local phase-space volume using the principal-axis directions following from the local linear approximation, after diagonalization by the solution of the eigenproblem in the units specified by the S' matrix. In the present context, the shape of the local sampling volume is that of a five-dimensional rectangular parallelepiped.

In practical computations, we need to discretize the interval of the mapping element and, after solving the five-dimensional local least-squares problem, interpolate the interval parameters for Eq. (2.11). Once the entire variation-interval map is available across the interval of the mapping parameter, trial orbits are generated in a straightforward way. First, a value for the mapping orbital element is obtained from uniform sampling over the mapping interval. Second, the remaining five elements are generated by interpolating their variation intervals based on the precomputed map. Third, the trial orbit qualifies

https://doi.org/10.1017/S1743921304008713 Published online by Cambridge University Press

for a sample orbit if it produces an acceptable fit to the observations. Each sample orbit is accompanied by the weight factor

$$w(P_{\rm m}, \boldsymbol{P}') \propto \sqrt{\det \Sigma^{-1}(P_{\rm m}, \boldsymbol{P}')} \cdot \exp\left[-\frac{1}{2}\chi^2(P_{\rm m}, \boldsymbol{P}')\right] \cdot \sqrt{\frac{\lambda_1(P_{\rm m}) \cdot \ldots \cdot \lambda_5(P_{\rm m})}{\lambda_1(P_{\rm m,ls}) \cdot \ldots \cdot \lambda_5(P_{\rm m,ls})}}. \tag{2.12}$$

2.3. *Statistical orbital ranging*

For initial orbit computation, we make use of Ranging (Virtanen *et al.* 2001, Muinonen *et al.* 2001). In Ranging, two observation dates (here A and B) are chosen from the complete observation set. The corresponding topocentric distances (or ranges $\rho_{\rm A}$ and $\rho_{\rm B}$), as well as the R.A. ($\alpha_{\rm A}$ and $\alpha_{\rm B}$) and Dec. ($\delta_{\rm A}$ and $\delta_{\rm B}$) angles are MC sampled using intervals subject to iteration, resulting in altogether 12 interval boundary parameters. Explicitly,

$$\begin{cases} \rho_{\rm A} & \in & [\rho_{\rm A}^-, \rho_{\rm A}^+], \\ \alpha_{\rm A} & \in & [\alpha_{\rm A}^-, \alpha_{\rm A}^+], \\ \delta_{\rm A} & \in & [\delta_{\rm A}^-, \delta_{\rm A}^+], \end{cases} \qquad \begin{cases} \rho_{\rm B} & \in & [\rho_{\rm A} + \rho_{\rm B}^-, \rho_{\rm A} + \rho_{\rm B}^+], \\ \alpha_{\rm B} & \in & [\alpha_{\rm A}^-, \alpha_{\rm A}^+], \\ \delta_{\rm B} & \in & [\delta_{\rm A}^-, \delta_{\rm A}^+]. \end{cases} \tag{2.13}$$

Note that it is computationally efficient to generate $\rho_{\rm B}$ based on $\rho_{\rm A}$ generated at an earlier stage. The boundary values $\rho_{\rm B}^{\pm}$ must be carefully chosen so as to secure the coverage of the entire relevant interval in $\rho_{\rm B}$. Once the two sets of spherical coordinates have been generated, the two corresponding Cartesian positions $(X_{\rm A}, Y_{\rm A}, Z_{\rm A})^T$ and $(X_{\rm B}, Y_{\rm B}, Z_{\rm B})^T$ lead to an unambiguous set of orbital elements $\boldsymbol{P}$, based on well-established techniques in celestial mechanics.

The set of trial orbital elements $\boldsymbol{P}$ is included in the set of sample orbital elements if and only if it produces an acceptable fit to the entire set of observations, that is, with the help of Eq. (2.3),

$$\exp\left[-\frac{1}{2}(\chi^2(\boldsymbol{P}) - \chi^2(\boldsymbol{P}_{\rm ref})) + \ln\sqrt{\det\Sigma^{-1}(\boldsymbol{P})} - \ln\sqrt{\det\Sigma^{-1}(\boldsymbol{P}_{\rm ref})}\right] \geqslant c_{\rm min}, \tag{2.14}$$

where $c_{\rm min}$ is the level of acceptance and $\boldsymbol{P}_{\rm ref}$ refers to the best-fit orbital solution available, constantly updated during the iterative computation. The acceptance criterion thus becomes analogous to the $\Delta\chi^2$ criterion for Gaussian p.d.f.'s (Eq. 2.6).

In order to establish the uniform sampling of orbital elements $\boldsymbol{P}$, each set of sample orbital elements is weighted by the Jacobian of the transformation from "the phase space" of the two spherical positions $(\rho_{\rm A}, \alpha_{\rm A}, \delta_{\rm A})^T$ and $(\rho_{\rm B}, \alpha_{\rm B}, \delta_{\rm B})^T$ to the phase space of the orbital elements,

$$w(\boldsymbol{P}) \propto \det\left[\frac{\partial(\rho_{\rm A}, \alpha_{\rm A}, \delta_{\rm A}; \rho_{\rm B}, \alpha_{\rm B}, \delta_{\rm B})}{\partial \boldsymbol{P}}\right]^{-1}. \tag{2.15}$$

Ranging is repeated to obtain a large number of sample orbits, simultaneously iterating the 12 interval boundary parameters and updating the reference orbital elements in order to secure the coverage of the full orbit solution space.

2.4. *Collision probability using 6D orbital-element p.d.f.'s*

Muinonen (1999) and Muinonen *et al.* (2001) described a set of techniques for the computation of the collision probability for Earth-crossing asteroids. Their formulation of

https://doi.org/10.1017/S1743921304008713 Published online by Cambridge University Press

the collision probability computation relies on the Bayesian a posteriori probability density function $p_{\rm p}$ of the orbital elements $\boldsymbol{P}$, from which the collision probability follows through the integral:

$$P_{\rm c}(\tau) = \int_{C(\tau)} d\boldsymbol{P}\, p_{\rm p}(\boldsymbol{P}, t_0), \tag{2.16}$$

where the phase space domain $C(\tau)$ contains the elements leading to a collision on the interval τ.

In particular, Muinonen *et al.* introduced new techniques for computing the collision probability for the case of short observational arcs and/or small numbers of observations. The orbital-element p.d.f. can in this case be very complicated, and it must be assessed rigorously using Monte Carlo simulations for large numbers of sample orbits. Once the extent of the orbital-element probability density has been mapped by generating a large, unbiased set of sample orbits, these orbits can be propagated through the assumed impact interval τ to derive the weighted fraction of collision orbits, i.e., the collision probability.

Even if none of the sample orbits lead to collision within the impact interval, the probability for a collision within the interval is not necessarily zero. This can simply mean that the sampling of the phase space for acceptable orbital solutions has not been dense enough. Either because, at an epoch close to the observations this 6D phase-space region is extremely large, as it is for short observational arcs, and it cannot be efficiently mapped keeping the sample size computationally reasonable. Or, if the time scale of propagation is very long, repeated close-approaches introduce chaotic effects causing the extent of an initially small phase-space volume (computed close to the epoch of the observations) to widen so that the sampling of the impact parameter space is, again, too sparse. In both cases, the result is that the impacting orbit solutions are missed, because they are typically confined to very narrow regions in the phase space.

The above limitations of the direct propagation of the orbital-element p.d.f. through the impact interval can be solved by changing from discretized p.d.f.'s to continuous functions using intervals of collision orbits (Muinonen *et al.*). In this method, intervals of acceptable orbits are computed in the vicinity of each sample orbital element set, and within these intervals a sub-interval is mapped including orbits that result in collision in the given time interval. The limitation of this method is that the computational load can easily become excessive when the unbiased orbital intervals are searched.

For robust and rapid evaluation of collision probability, Muinonen et al. provided upper bounds in terms of maximum likelihood (ML) collision orbit. This can be determined once collision orbits have been found in the neighborhood of the orbit maximizing the orbital-element p.d.f., i.e., around the maximum likelihood orbit. The ML collision orbit is then the collision orbit that lies probabilistically closest to the ML orbit. However, the upper bound values have been shown to give only loose bounds to the collision probability, so more rigorous means should be used whenever the more severe computational load can be handled.

3. Results and discussion

The orbital-element p.d.f. is here assessed using the two techniques described in the previous section. Ranging has proven to be a practical way to assess the probability density for objects with very short observational arcs, while the new VOV sampling has turned out useful for the moderately observed ones. For well-observed objects, we use the standard least-squares covariances to estimate the widths of the orbital-element p.d.f.'s.

https://doi.org/10.1017/S1743921304008713 Published online by Cambridge University Press

For collision risk assessment, we applied the most simple approach described in the previous section: the direct propagation of the orbital-element p.d.f. through the predicted impact interval. In what follows, we will see that this turned out to be the first time that the collision risk could indeed be estimated directly using sample collision orbits. During the integrations, we also monitor for (temporary) satellite captures and Earth swing-by's to hyperbolic orbits as well as impacts to the Moon.

3.1. *2004 AS$_1$*

The Apollo asteroid 2004 AS$_1$ grabbed the attention of asteroid scientists for several days in January 2004 when, based on single-night data from only one observatory, this asteroid appeared to be on a collision course with the Earth with the timing of the predicted impact only about 48 hours after the discovery. Although the risk of immediate impact was ruled out as soon as the follow-up observations from the second night came in, the extreme nature of the first prediction called for a detailed analysis. First, we present the results for orbit computations, then we return to the analysis of the actual collision probability.

3.1.1. *Phase transition*

To locate the phase transition regime, we carried through the following orbit computation scheme using methods described in Section 2. As already implied by the preliminary study in Muinonen and Virtanen (2002) in the case of improving observational accuracy, the occurence of this nonlinear collapse in the orbital distributions is most likely highly case-sensitive. Thus, pinpointing its exact location for each object requires breaking down of the object's observational data night by night and applying the different statistical methods to the data in a sequential manner.

For 2004 AS$_1$, we considered the observational data for the first month after discovery which we divided into the following seven cases in the order of increasing time arc: 0.04 ($\sim$ 1 hr), 1.1, 1.5, 3.0, 5.0, 8.0, and 30.0 days. Ranging was applied to the five first cases, i.e., up to 5 days of observations, VOV-sampling from the third arc onwards (1.5 days) and least-squares fit from 1.1 days onwards. The resulting orbital-element p.d.f.'s are compared in Figure 1 where we plot for the semimajor axis the standard deviations of the marginal p.d.f.'s obtained with the different techniques.

The phase transition regime extents from the discovery night (1 hr arc) to the second night of observations, with the most abrupt collapse taking place between arcs of 1.1 and 1.5 days. Across this regime, the orbital uncertainties decrease by several orders of magnitudes for all the elements, but the improvement is most significant for the semimajor axis, close to a factor of 10^5. It is notable that for this NEO, for the semimajor axis, the uncertainties based on the linear technique, i.e., the least-squares covariances, are in good agreement with the ones from rigorous nonlinear techniques.

3.1.2. *Collision risk at discovery*

The discovery night observations of 2004 AS$_1$ consisted of four observations over 1 hour from a single observatory. The first published ephemerides by the Minor Planet Center (MPC) showed a rapid increase in the apparent brightness and indicated that this asteroid would indeed be passing within the Earth radius some 48 hours later. Although the orbit solution behind this prediction was quickly replaced by another equally acceptable solution at the MPC (resulting in ephemerides that no more passed through the planet), it was not before the new observations from the second night came in that the possibility for an immediate (and future) impact could be overruled. Further observations in the following months finally showed that the accuracy of the four initial observations was

https://doi.org/10.1017/S1743921304008713 Published online by Cambridge University Press

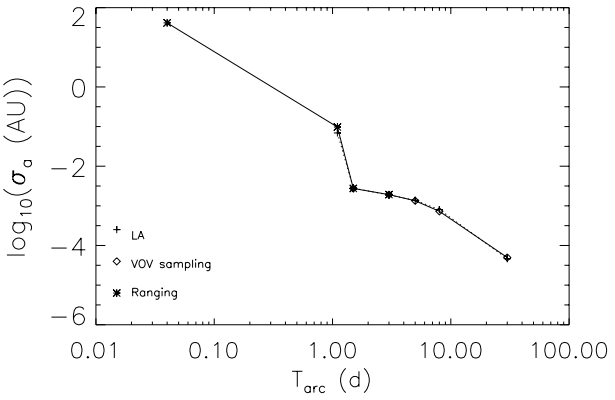

Figure 1: Phase transition in the accuracy of the semimajor axis as a function of the increasing observational arc for 2004 AS_1 (obs. accuracy ~ 0.5 arcsec). Note the logarithmic scale on the vertical axis. LA stands for linear approximation, i.e., 6D covariances of the least-squares solutions.

rather poor (rms-values of 1.4 and 1.3 arcseconds for R.A. and Dec.) and that one observation was clearly an outlier (residuals of 2.4 and 1.9 arcseconds for R.A. and Dec.). The overall evolution of this case raised several questions: what was the effect of discordant observations in collision probability assessment? Can outliers be recognized from very short arcs? How did the collision probability estimates evolve as the observational arc increased?

We used the Ranging technique to map the 6D orbital element p.d.f. at discovery with 50,000 sample orbits. As the first orbit solution used by the MPC led to a collision, it seemed a priori evident that collision orbits would be among the best-fit orbit solutions. The collision risk was thus estimated by deriving the impact parameter distribution by propagating the 50,000 orbits through the iterated impact interval of January 14 to 17, 2004. We first made a conservative assumption of 1.0 arseconds for the observational noise. The collision risk is illustrated with the cumulative distribution function (c.d.f.) for the impact parameter in Figure 2, which confirms the drastic first prediction: for 1.0 arcsecond noise, the probability for an Earth impact was 12 %, several orders of magnitude higher than any of the previously estimated asteroid impact risks.

We then repeated the analysis (orbit and impact parameter computation) for different assumptions of the observational noise: 2.0, 1.5, 0.5, and 0.3 arcseconds. The evolution of collision risk as a function of the noise assumption is shown in Figure 3a: when the observations are assumed more accurate, the impact probability increases. The reason can be found by looking at the results from Ranging: assumption that the data was more accurate (less affected by noise) made the asteroid's plausible topocentric range interval to concentrate towards the Earth. This again shows that the best-fit orbits actually led to collisions within the predicted interval.

To study the evolution of collision risk as a function of time, we added one simulated observation to the data set: since the collision risk vanishes after the second night of observations, simulated observation was propagated between the first and second night. This study implies that a fifth observation 30 minutes after the last one in the original data set (increasing the time arc from 1 to 1.5 hr) could already have made the difference and removed the impact risk.

https://doi.org/10.1017/S1743921304008713 Published online by Cambridge University Press

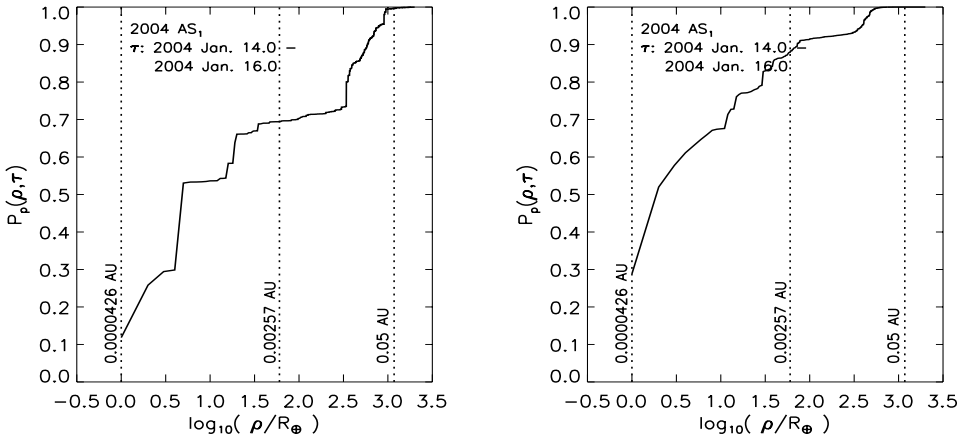

Figure 2: Collision risk with the Earth for 2004 AS$_1$ during January 14-17, 2004. Impact parameter c.d.f.'s have been computed with different assumption of the observational rms: 1.0 arcsec (left) and 0.5 arcsec (right). The estimates for the collision risk are 12% and 28%, respectively.

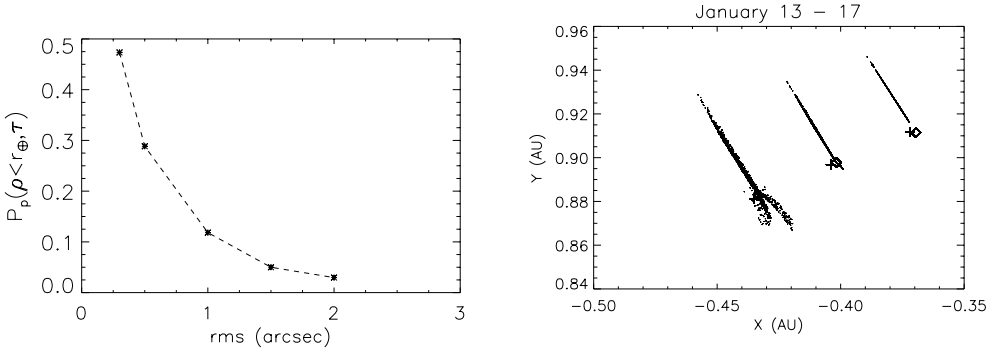

(a) (b)

Figure 3: **a)** Evolution of the collision risk for 2004 AS$_1$ as a function of the assumed observational rms. **b)** Evolution of the positional uncertainty for 2004 AS$_1$ in the ecliptic plane during the assumed impact interval. Position distributions are shown for the following dates (from right to left): January 13th, 15th and 17th. Positions of Earth and Moon are shown with diamond and cross, respectively.

As to the effect of the discordant observations, first, the distributions of residuals from Ranging technique (cf. Fig. 7 in Bowell *et al.* 2002) did not reveal the outlier, although there were indications that the observations in general were not very accurate. Second, removing one observation at a time and repeating the above analysis for collision risk did not have major impact to the estimated values. Thus, the presence of discordant observations could not be deduced from the initial data.

Finally in Figure 3b, we show the highly nonlinear nature of the impact event with the evolution of the positional uncertainty over the impact interval. The close approaches to the Earth have scattered the position distribution of 2004 AS$_1$ significantly at the post-impact epoch of January 17, 2004 (left-most cloud of points).

https://doi.org/10.1017/S1743921304008713 Published online by Cambridge University Press

4. Conclusions

We have applied our spectrum of statistical orbit computation techniques for 2004 AS_1 to study the evolution of orbital uncertainties as a function of time. We find that the nonlinear phase transition in the orbital p.d.f.'s for this asteroid takes place after 1.5 days of observations. We will continue to study the phase transition in more detail for different populations of minor planets, paying also attention to the case of high-precision astrometry obtained, e.g., from future space missions, such as the European Space Agency's GAIA space observatory. The succesful application of VOV technique and the consistency of the results with Ranging indicates that the new technique will be useful at the phase transition regime.

We confirm the extreme initial estimates for the collision risk of 2004 AS_1 for the time span of January 14-17. 2004. The risk of collision based solely on the discovery night data was indeed non-vanishing, estimates as high as 50% resulted from our analysis. However, we note that the strict probabilistic interpretation of both the inverse and prediction problem may no longer be valid for such exiguous data, and the probability values should be taken as loose estimates only. We investigate the use of regularizing a priori probability density further and present a more complete collision risk analysis for this case study in Virtanen *et al.* 2004.

Acknowledgements

The research is supported by the Finnish Graduate School in Astronomy and Space Physics and by the Academy of Finland.

References

Bowell, E., Wasserman, L.H. & Muinonen, K. 1993, *Bull. Am. Astron. Soc.* 25, 1118

Bowell, E., Virtanen, J., Muinonen, K. & Boattini, A. 2002, in: W.F. Bottke Jr., A. Cellino, P. Paolicchi & R.P. Binzel (eds.), *Asteroids III*, p. 27

Chodas, P.W. & Yeomans, D.K. 1996, in: K.S. Noll, H.A. Weaver & P.D. Feldman, (eds.), *The Collision of Comet Shoemaker-Levy 9 and Jupiter*. (Cambridge University Press)

Chodas, P.W. & Yeomans, D.K. 1999, in: *2*1st Annual AAS Guidance and Control Conference, Paper 99-002

Jeffreys, H. 1946, *Proceedings of the Royal Statistical Society of London, Series A* 186, 453

Milani A. 1999, *Icarus* 137, 269

Milani, A. & Valsecchi, G.B. 1999, *Icarus* 140, 408

Milani, A., Chesley, S.R. & Valsecchi, G.B. 1999, *Astron. Astrophys.* 346, L65

Milani, A., Chesley, S.R. & Valsecchi, G.B. 2000, *Planet. Space Sci., ACM'99 Special Issue*, Vol. 48, 945

Milani, A., Chesley, S.R., Boattini, A., Valsecchi, G.B. & Giovanni, B. 2000, *Icarus* 144, 12

Milani, A., LaSpina, A., Sansaturio, M.E. & Chesley, S.R. 2000, *Icarus* 144, 39

Muinonen, K. & Bowell, E. 1993, *Icarus* 104, 255

Muinonen, K. 1999, in: A.E. Roy & B.A. Steves (eds.), *The Dynamics of Small Bodies in the Solar System: A Major Key to Solar System Studies* (Kluwer), p. 127

Muinonen, K., Virtanen, J. & Bowell, E. 2001, *Cel. Mech. Dyn. Astron.* 81, 93

Muinonen, K. & Virtanen, J. 2002, in: S. Isobe & Y. Asakura (eds.), *International Workshop on Collaboration and Coordination Among NEO Observers and Orbital Computers*, p. 105

Muinonen, K., Virtanen, J., Granvik, M. & Laakso, T. 2004, *Mon. Not. R. Astron. Soc.*, to be submitted

Virtanen, J., Muinonen, K. & Bowell, E. 2001, *Icarus* 154, 412

Virtanen, J. & Muinonen, K. 2004, *Icarus*, submitted